Published in Journal of Optical Society of America A, 38, 9, 1357-1365 (2021)

Analysis of Mie resonances using the Debye series

PHILIP LAVEN

9 Russells Crescent, Horley, RH6 7DJ, United Kingdom
philip@philiplaven.com

Scattering of light from homogeneous spherical particles can exhibit sharp resonances as functions of particle size, wavelength or refractive index. Such resonances, usually known as morphology-dependent resonances (MDRs) or whispering gallery modes (WGMs), have been exhaustively studied using Mie theory for many years. This paper demonstrates that the Debye series expansion provides a succinct and easily-understood representation of these resonances: for example, the Debye coefficient $R^{121}{}_n$ determines (a) the exact conditions for resonance, (b) the number of terms required to replicate the Mie result and (c) the Q factor of the resonance.

1. INTRODUCTION

Scattering of light from homogeneous spherical particles can exhibit sharp resonances [1-19], often known as morphology-dependent resonances (MDRs) or whispering gallery modes (WGMs). Such resonances are very dependent on particle size, wavelength and refractive index.

Most theoretical studies of these resonances have been based on Mie calculations, but this paper employs the Debye series expansion [20-22]. The Debye series can be used to identify scattering contributions of order p. The $p = 0$ term corresponds to diffraction and external reflection, whereas the $p = 1$ term represents transmission through the sphere. Terms with $p > 1$ correspond to waves that have been subjected to $p - 1$ internal reflections. Despite its similarity to geometrical optics, it must be emphasized that the Debye series is not an approximation: the sum of the terms from $p = 0$ to $p = \infty$ gives exactly the same result as the Mie calculation. Some studies of resonances [9, 13-14] have used the Debye series to remove the background scattering caused by specific dominant low-order terms (such as $p = 2$ and $p = 11$), thus revealing the resonances more clearly.

The overall aim of this paper is to examine the role of the entire Debye series in the formation of resonances. Section 2 of this paper reviews the properties of these resonances based Mie calculations. Section 3 analyzes the number of terms in the Debye series needed to approximate the Mie results near some example resonances. Section 4 analyzes the amplitudes and phases of the scattering contributions from individual terms of the Debye series in the vicinity of resonances. Section 5 highlights the importance of the coefficient $R^{121}{}_n$ in the Debye series expansion in determining the characteristics of individual resonances. Section 6 offers some conclusions.

2. MIE CALCULATIONS

In Mie calculations, the scattering amplitudes $S_1(\theta)$ and $S_2(\theta)$ for TE and TM polarizations respectively are obtained by the partial wave sums:

$$S_1(\theta) = \sum_{n=1}^{n_{\max}} \{(2n+1) / [n\,(n+1)]\}\,[a_n\,\pi_n(\theta) + b_n\,\tau_n(\theta)] \quad (1a)$$

$$S_2(\theta) = \sum_{n=1}^{n_{\max}} \{(2n+1) / [n\,(n+1)]\}\,[a_n\,\tau_n(\theta) + b_n\,\pi_n(\theta)] \quad (1b)$$

where the angular functions are:

$$\pi_n(\theta) = [1/\sin(\theta)]\,P_n^1[\cos(\theta)] \quad (2)$$

$$\tau_n(\theta) = (d/d\theta)\,P_n^1[\cos(\theta)] \quad (3)$$

Mie resonances are clearly visible in Fig. 1 which plots $|S_1(\theta)|$ for the arbitrary scattering angle $\theta = 150°$ as a function of size parameter $x = 2\pi r/\lambda$, where r is the radius of the homogeneous sphere of refractive index $m = 1.3333$ and λ is the wavelength of the incident light.

Resonances can be characterized by n (the partial wave number) and by l (the number of radial modes), as indicated at the top of Fig. 1. Some of the resonances (e.g. at $x = 98.1312$ and $x = 98.1932$) coincide with local maxima of $|S_1(\theta)|$, whereas other resonances (e.g. at $x = 99.2567$) coincide with local minima. The resonances at $x = 98.4732$ and $x = 99.7511$ have a local minimum and a local maximum.

The Mie results shown in Fig. 1 have been re-plotted in Fig. 2 as a parametric curve plotting $|S_1(\theta)|$ together with the phase ϕ of $S_1(\theta)$. The parametric curve includes several near-circular features, each of which seems to be associated with one of the Mie resonances shown in Fig. 1. Another oddity is that each of the resonances is positioned at the extreme left or extreme right of these nearly-circular features.

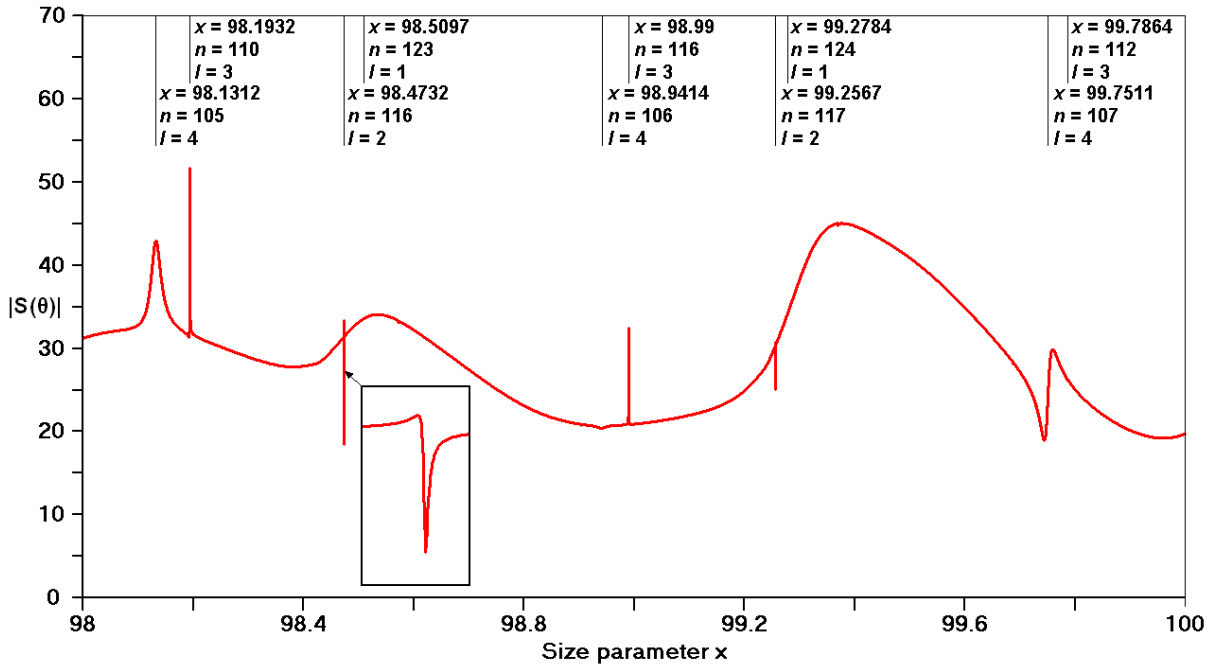

Fig. 1 Results of Mie calculations of scattering amplitude $|S_1(\theta)|$ at scattering angle $\theta = 150°$ as a function of size parameter x for a spherical particle of refractive index $m_1 = 1.3333$ in a medium of refractive index $m_2 = 1$ calculated at intervals of $\Delta x = 10^{-6}$. The parameters of each resonance (partial wave number n and radial mode l) are shown at the top of the graph. The inset box shows the resonance at $x = 98.4732$ in much greater detail. The resonances at $x = 98.5097$ ($n = 123$, $l = 1$) and $x = 99.2784$ ($n = 124$, $l = 1$) do not appear on the red curve because (a) the widths of these resonances are less than Δx and (b) the Mie calculations according to Eq. 1(a) have been terminated at $n_{max} = x + 4.05\, x^{1/3} + 2 \approx 121$.

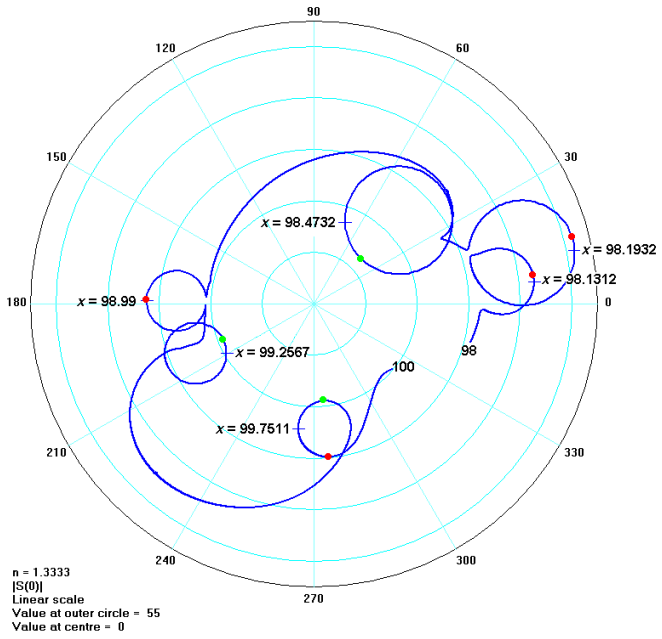

Fig. 2 Using the same conditions as Fig. 1 except that $\Delta x = 5 \times 10^{-8}$, the Mie results are shown as a parametric curve from $x = 98$ to $x = 100$ showing the amplitude and phase of $S_1(150°)$. The marked values of x correspond to the resonances shown in Fig. 1. Detailed inspection of the path followed by the blue curve identifies local maxima of $|S_1(150°)|$ (indicated by red dots) and local minima of $|S_1(150°)|$ (indicated by green dots).

Fig. 2 reinforces the idea that some Mie resonances can appear as local maxima, local minima or both. Following the curve in Fig. 2 starting at $x = 98$, the first resonance occurs at $x = 98.1312$ slightly before the red dot which indicates a local maximum. The next resonance at $x = 98.1932$ occurs just before another red dot at $x \approx 98.19321$ corresponding to a local maximum. The next resonance at $x = 98.4732$ is near a green dot corresponding to a local minimum. Similarly, the resonance at $x = 98.99$ coincides with a local maximum, whilst the resonance at $x = 99.2567$ is very near to a local minimum. However, the resonance at $x = 99.7511$ is accompanied by a local minimum at $x = 99.7444$ and a local maximum at $x = 99.7594$.

It has long been known [3-7] that TM and TE resonances of order n are respectively associated with the a_n and b_n terms in the Mie calculations. This is illustrated in Fig. 3 which shows that the TE resonance at $x = 98.1312$ ($n = 105$, $l = 4$) is due to the b_{105} term, whereas the TE resonance at $x = 98.1932$ ($n = 110$, $l = 3$) is due to the b_{110} term. Furthermore, Fig. 4 confirms that these resonances coincide with the imaginary part of b_n being zero (in both cases, the value of b_n is 1).

The calculations reported in this paper have been made for $\theta = 150°$, but the amplitudes of TE resonances as a function of θ are determined by the term $b_n\, \tau_n(\theta)$ in Eq. 1(a) with $b_n = 1$ at resonance. As an example, Fig. 5 plots $S_1(\theta)$ for $140° \le \theta \le 150°$ for the $n = 110$ resonance. As $\tau_n(\theta)$ is real, $S_1(\theta)$ is also real with positive and negative local maxima. Note that the $n = 110$ resonance disappears at certain values of θ, such as $\theta \approx 149.46°$ and $\theta \approx 151.09°$.

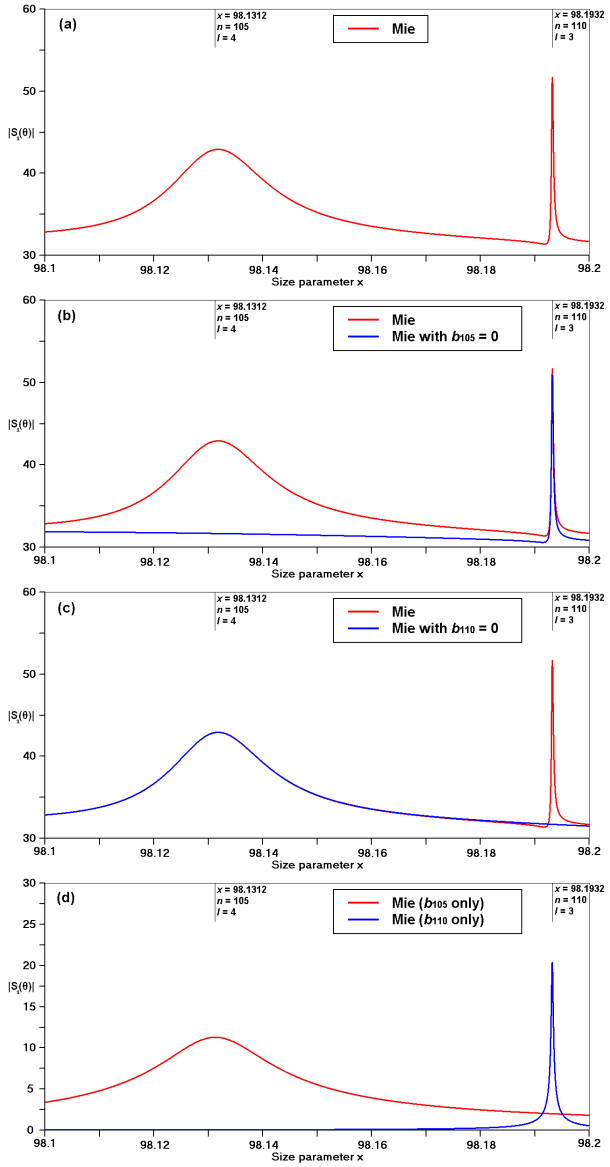

Fig. 3 (a) Mie results for $S_1(150°)$ showing a broad resonance at x = 98.1312 (n = 105, l = 4) and a narrow resonance at x = 98.1932 (n = 110, l = 3). (b) Setting b_{105} = 0 in the Mie calculation removes the broad resonance. (c) Setting b_{110} = 0 removes the narrow resonance. (d) The two resonances are caused by the b_{105} and b_{110} terms respectively.

3. THE DEBYE SERIES

The Debye series [20-22] defines the values of a_n and b_n used in Eqs. (1a) and (1b) in a form that isolates specific scattering mechanisms of order p, as shown in Eq. (4) below:

$$a_n, b_n = (1/2)\,[1 - R^{212}{}_n - \sum_{p=1}^{\infty} T^{21}{}_n\,(R^{121}{}_n)^{p-1}\,T^{12}{}_n] \qquad (4)$$

As Mie resonances seem to be the combined result of many terms in the Debye series (rather than being caused by a single value of p), it is not immediately obvious how the Debye series can be used to analyze Mie resonances.

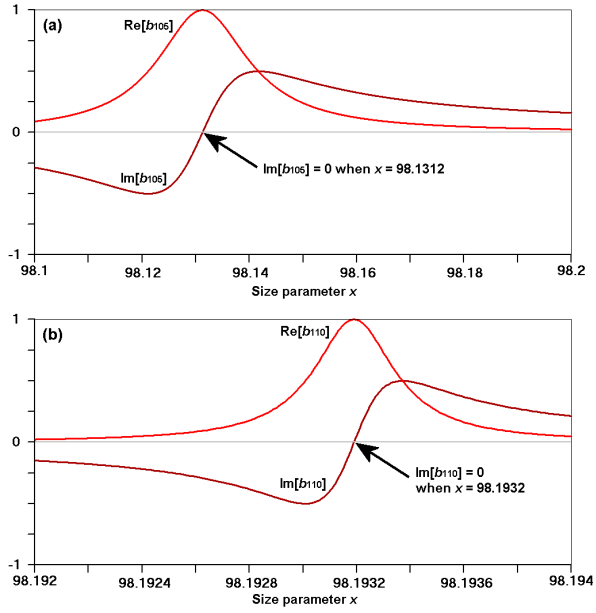

Fig. 4 (a) The broad resonance at x = 98.1312 (n = 105, l = 4) occurs when the imaginary part of b_{105} = 0. (b) The narrow resonance at x = 98.19319 (n = 110, l = 3) occurs when the imaginary part of b_{110} = 0.

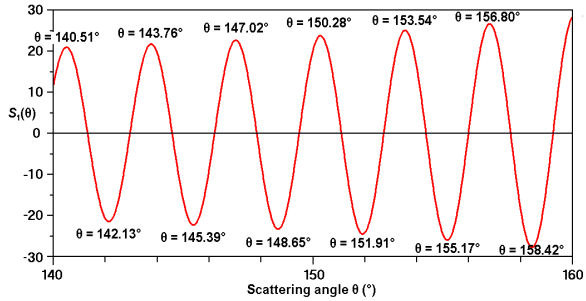

Fig. 5 Graph of $S_1(\theta)$ for the n = 110 resonance as a function of θ. Note that $S_1(\theta)$ is real, with positive and negative maxima separated by about 1.63°.

One approach is shown in Fig. 6, which compares the Mie results (shown in red) with the sum of the Debye series contributions (shown in blue) for p = 0 through $p = p_{\max}$ for various values of $p_{\max}$. If the Mie results exactly matched the Debye series results, the red lines would not be visible because they would have been overwritten by the blue lines.

Fig. 6(a) shows that the match is far from perfect for $p_{\max}$ = 100: the blue line reproduces the general trend of the red line in the vicinity of the broad resonance at x = 98.1312, but it entirely misses the narrow resonance at x = 98.1932. Figs. 6(b)-(f) demonstrate that increasing the value of $p_{\max}$ for the Debye series gives progressively closer matches to the Mie result. In particular, Fig. 6(b) shows that the broad resonance at x = 98.1312 can be approximated by the first 200 terms of the Debye series, but Fig. 6(f) suggests that the narrow resonance at x = 98.1932 requires slightly more than 10,000 terms of the Debye series.

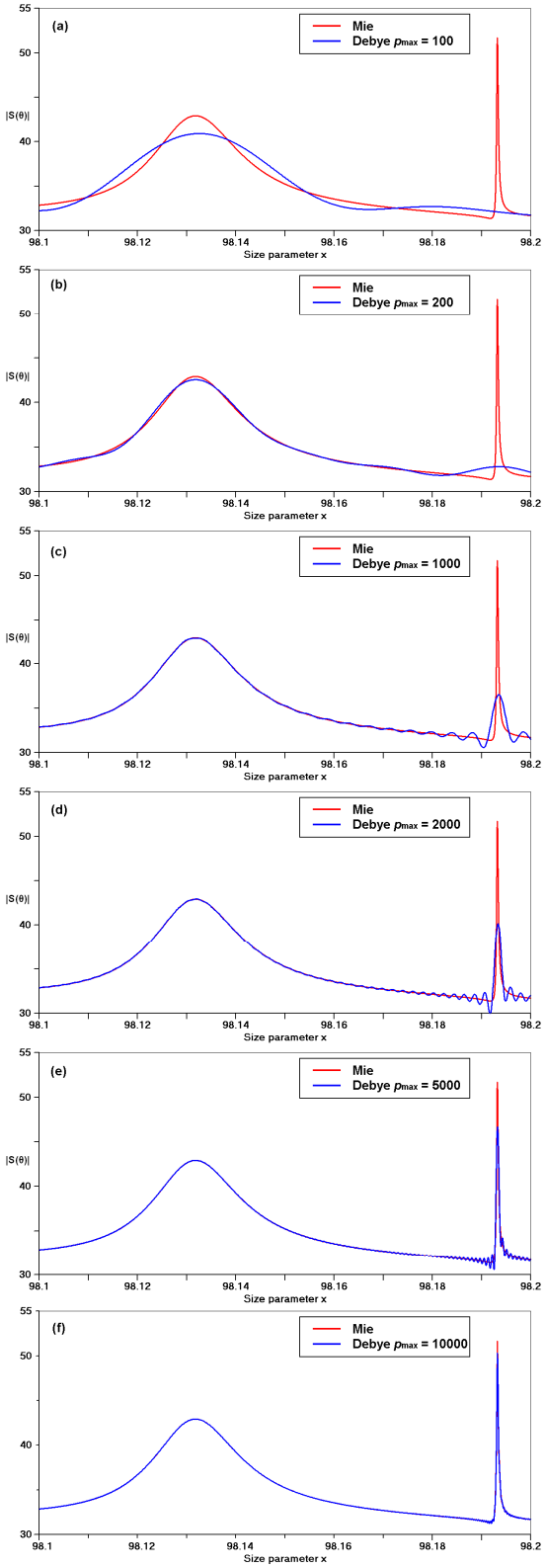

Fig. 6 Comparisons of Mie results for $S_1(150°)$ with the Debye series contributions from $p = 0$ through $p = p_{max}$. The broad resonance at $x = 98.1312$ can be closely approximated by using the first 200 terms of the Debye series, but the narrow resonance at $x = 98.1932$ requires slightly more than 10,000 terms.

4. ANALYSING THE DEBYE SERIES

Fig. 7 displays the Debye series results in an entirely different way: each dot plots the value of $S_1(\theta)$ in terms of its magnitude $|S_1(\theta)|$ and phase ϕ for $x = 98.1$ and $\theta = 150°$ for every value of p from $p = 0$ to $p = 20{,}000$. This diagram also shows the Mie result at $|S_1(\theta)| = 32.9$ and $\phi = 357.9°$. The dominant contributions to the Mie result are from the $p = 2$, $p = 0$ and $p = 7$ terms in the Debye series. The dots are also color-coded in accordance with the scale shown to the right of Fig. 7. The arrangement of the colors of the dots in the diagram suggests that, when p is large, the amplitudes of the contributions generally decrease as p increases, but careful examination indicates that there are many exceptions to this rule. Although Fig. 7 shows Debye series results for values of $p \leq 20{,}000$, Fig. 6(b) shows that $p_{max} = 200$ is sufficient to reproduce the Mie result when $x = 98.1$. Looking at Fig. 7, it is clear that the phases of the high-order terms are distributed between 0° and 360°. If they were distributed uniformly in terms of phase, destructive interference would occur because a contribution with phase ϕ would be cancelled by another contribution of similar amplitude with phase $\phi \pm 180°$. In such cases, the high-order terms would have no effect on the sum.

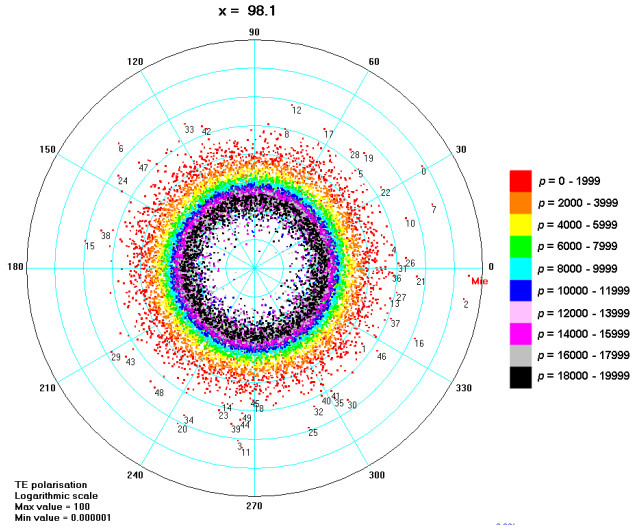

Fig. 7 Results for $x = 98.1$ and $m_1 = 1.3333$ in which the dots represent the amplitude and phase of the contributions to $S_1(150°)$ for every term in the Debye series from $p = 0$ through $p = 20{,}000$. The dots corresponding to $0 \leq p \leq 50$ have been identified by the value of p. The colors of the dots indicate the value of p according to the scale at the right of the diagram. The Mie result is also shown at $|S_1(150°)| = 32.9$ with phase $\phi = 357.9°$.

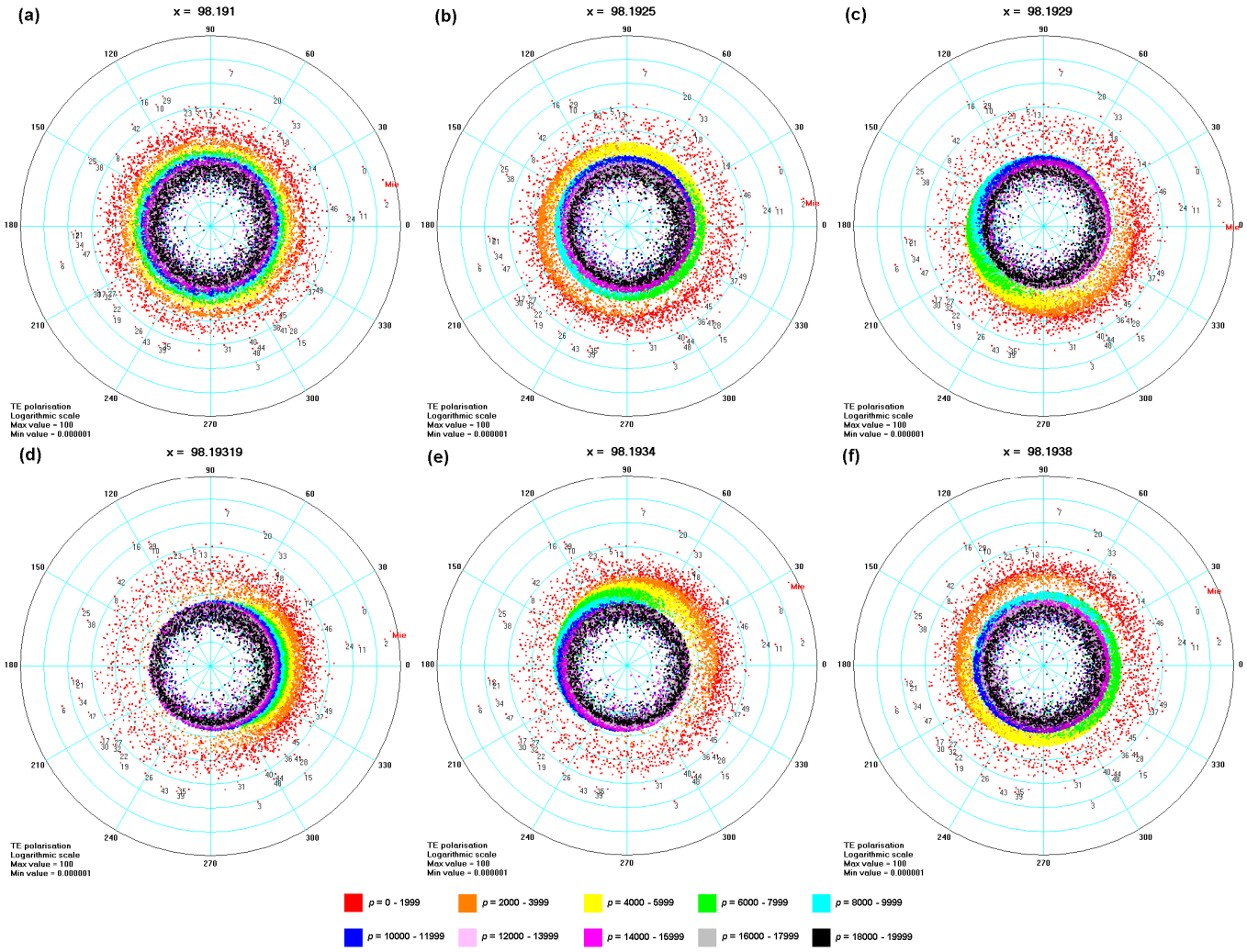

Fig. 8 As Fig. 7 but showing results for values of x in the vicinity of the resonance at x = 98.19319. Note that the colored dots seem to appear as a clockwise spiral when x < 98.19319 and as a counterclockwise spiral when x > 98.19319. **Supplemental Material**: A more detailed animated version of this figure is available at http://www.philiplaven.com/Fig_8.html.

The value of x = 98.1 used in Fig. 7 was selected because it is not near a Mie resonance. What happens near Mie resonances? Fig. 8 is a set of diagrams similar to Fig. 7 illustrating the effects on the amplitudes and phases of the Debye series contributions for $0 \le p \le 20{,}000$ as x is increased from 98.191 to 98.1938. The amplitudes do not seem to vary much, but the individual phases change dramatically near the (n = 110, l = 3) resonance at x = 98.19319 where the phases of the Debye terms seem to "congregate" together. Very few of the dots are in the left side of Fig. 8(d) (i.e. with phases between 90° and 270°) compared with those in the right side (i.e. with phases between 270° and 360° or between 0° and 90°). Examination of Fig. 8(d) suggests that this concentration is very pronounced for the yellow dots (representing Debye series terms with $4{,}000 \le p \le 5{,}999$), the green dots ($6{,}000 \le p \le 7{,}999$) and the cyan dots ($8{,}000 \le p \le 9{,}999$). This impression is confirmed by Fig. 9(a) in which the phases of the Debye series contributions for x = 98.19319 have been plotted as a function of p. This diagram shows a startling absence of red dots in the zone centered on ϕ = 180° and $p \approx 6{,}000$. As demonstrated in Fig. 3, the b_{110} term is responsible for this particular resonance. The phases of the b_{110} contributions are plotted as blue dots in Fig. 9(a) appearing as a blue straight line very close to 360°.

The amplitudes of the Debye series contributions are plotted as a function of p in Fig 9(b). The red dots show no obvious pattern as a function of p, but the straight blue line shows that the contributions from the b_{110} term reduce with each successive value of p. However, Fig. 9(b) also shows that the contributions from the b_{110} term are dominant when $p \approx 6000$. As shown by Fig. 9(a), all of the b_{110} contributions have phases close to 360°, thus explaining why the red dots in Fig. 9(a) are clustered around 360° (or 0°) when the b_{110} contributions are dominant.

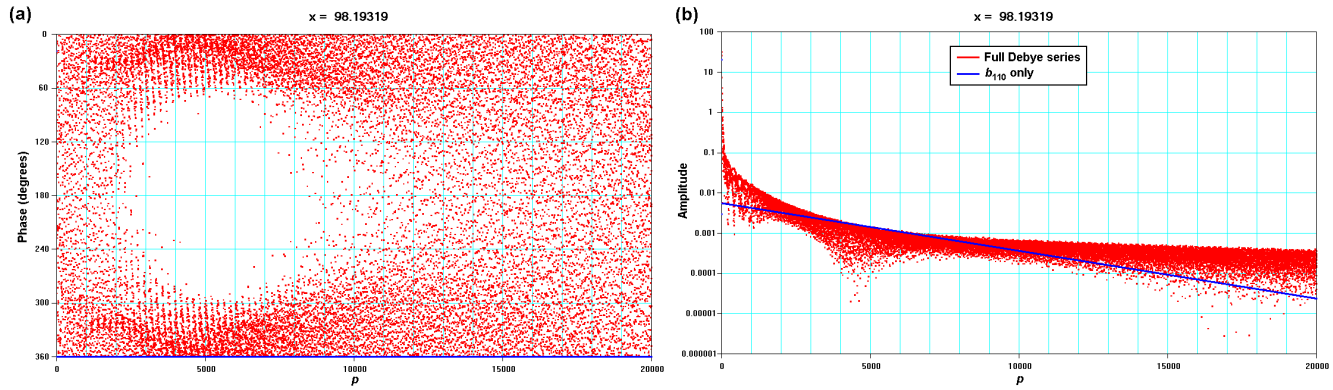

Fig. 9 Plots of the Debye series contributions to $S_1(150°)$ for the n =110 resonance at x = 98.19319 as a function of p showing (a) the phases and (b) the amplitudes. The red dots show results from all partial waves, whereas the blue dots show only results from the b_{110} term corresponding to the n =110 partial wave.

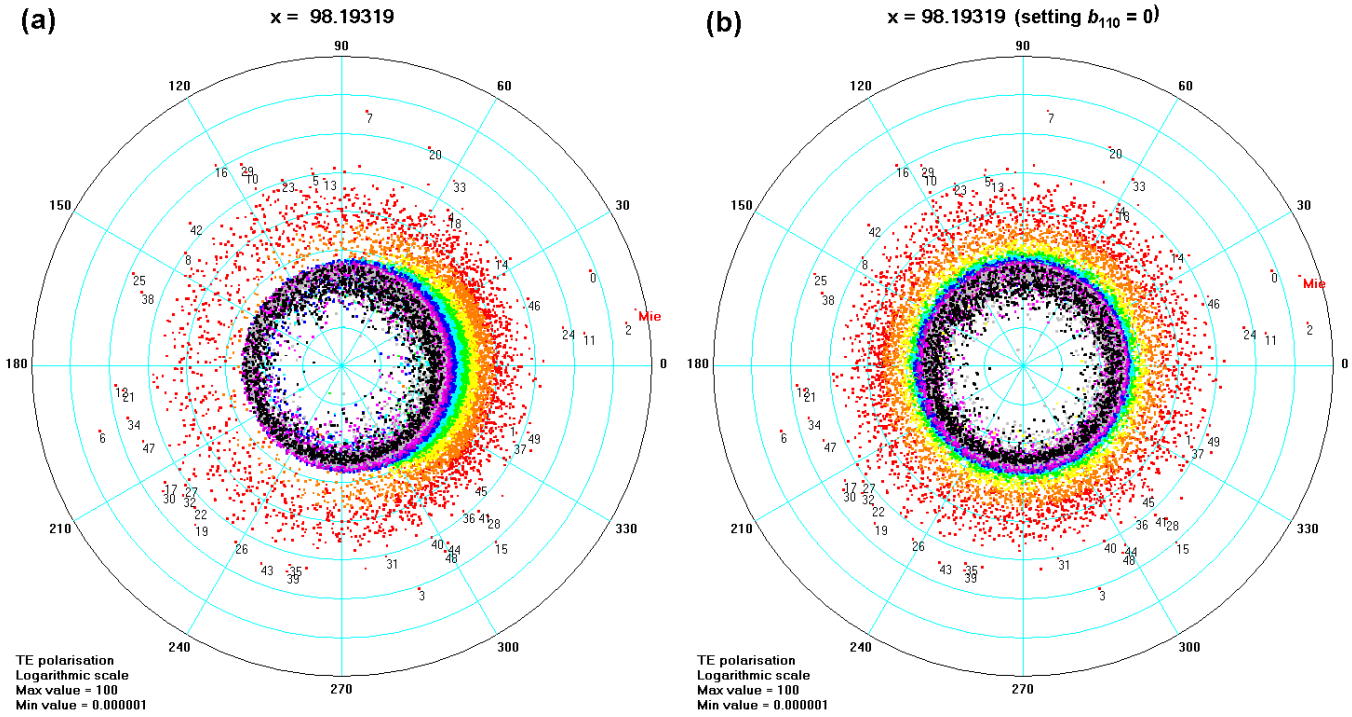

Fig. 10 Calculations for x = 98.19319 in which the dots represent the amplitudes and phases of the contributions to $S_1(150°)$ from every term in the Debye series from p = 0 through p = 20,000 (using the color scale shown in Fig. 7). Diagram (a) shows results from the full Debye series, together with the Mie result at $|S_1(150°)|$ = 51.47 and ϕ = 11.04°, whereas (b) shows results obtained by setting b_{110} = 0, with the Mie result at $|S_1(150°)|$ = 31.72 and ϕ = 18.13°.

Fig 10 explores the effects of the b_{110} term on the Debye series results at this resonance: Fig. 10(a), which is an enlarged version of Fig. 8(d), is very different to Fig. 10(b) where the b_{110} term has been set to zero. The uneven distribution in Fig. 10(a) is obviously caused by the b_{110} term.

The results shown in Fig. 10 have been combined in Fig. 11 by plotting the cumulative contribution made by each term p in sequential order starting from p = 0 though p = 20,000. Results for the full Debye series are given in Fig. 11(a), which includes an extraordinary horizontal line pointing towards the Mie theory result. In essence, Fig. 11(a) is the sum of the two parts of Fig. 11(b) – demonstrating that the horizontal line is caused by the b_{110} term, corresponding to the partial wave n = 110.

Fig. 11(a) identifies the dominant p = 0, 2, 3, 6 and 7 terms, as well as showing that very high-order terms are responsible for the horizontal line. On the other hand, the upper part of Fig. 11(b) shows that terms with p > 200 make no significant contribution to the pattern when b_{110} = 0. The fact that the multi-colored lines in Fig. 11 (a) and (b) are straight when p is large suggests the scattering contributions from different values of p are in phase. As these lines are also horizontal, it seems that the average phase of these contributions is very close to 0°.

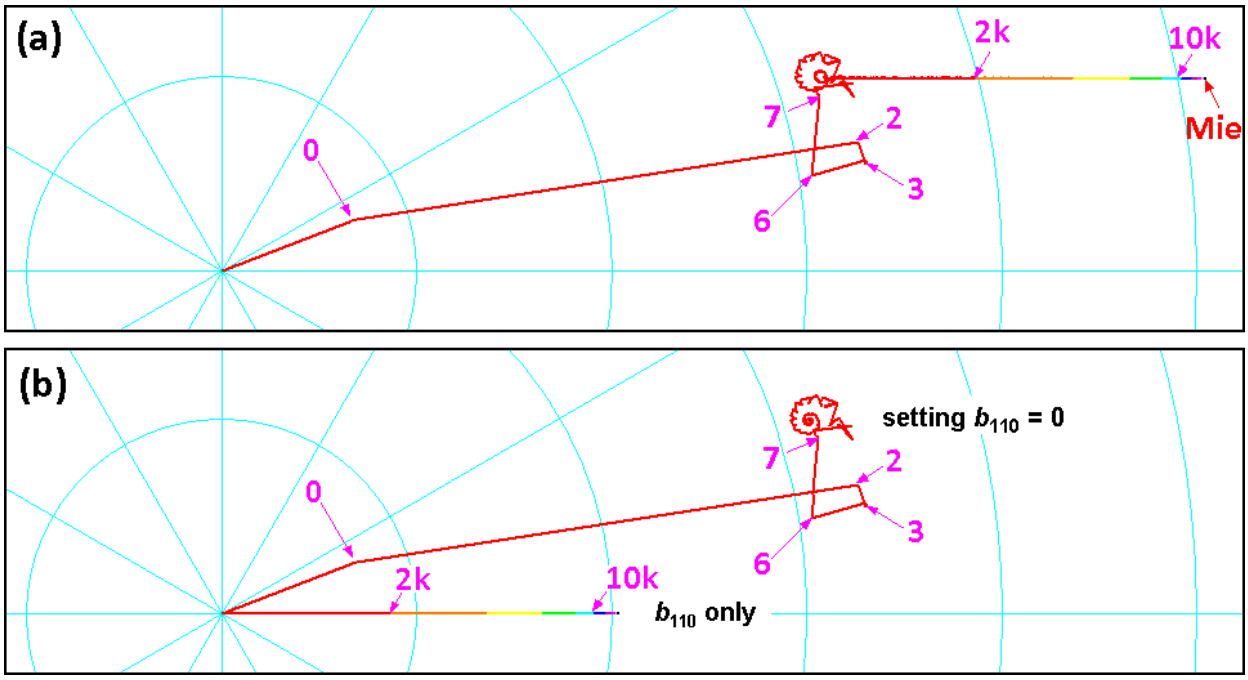

Fig. 11 The cumulative sum of the Debye series contributions to $S_1(150°)$ in sequential order of p have been plotted using a linear scale for x = 98.19319. Diagram (a) plots results from the Debye series for all partial waves, showing how increasing the value of p up to 20,000 causes the Debye result to approach the Mie result of $|S_1(150°)|$ = 51.47 and ϕ = 11.04°. The multi-colored line in (b) shows the Debye results for p up to 20,000 due solely to the partial wave n = 110. The upper curve in (b) shows that partial waves other than n = 110 are responsible for the dominant low-order terms (e.g. p = 0, p = 2 and p = 7) but they make no significant contribution when p > 200.

Fig. 9 demonstrated that, even at resonance, the phases of the very high-order terms for the full Debye series are typically not close to 0°. This anomaly is evident in Fig. 12 which is a much-magnified version of the straight line in Fig. 11(a) for values of $p \approx$ 18,000, demonstrating that the contributions made by individual values of p exhibit dramatic variations in amplitude and phase. By comparison, the straight line in the lower part of Fig. 11(b) is very well-behaved since all of the contributions from the p terms are precisely in phase, resulting in a smooth straight line. Despite the detailed differences in shape, the two sets of horizontal lines in Fig. 11 have the same overall length, confirming that the net effect of contributions with p > 200 is zero when the b_{110} term is ignored.

Recalling that Fig. 11 has been calculated for the resonance condition at x = 98.19319, Fig. 13 shows what happens at other values of x close to this resonance. Note that the multi-colored lines display clockwise spirals when x < 98.19319 and counterclockwise spirals when x > 98.19319. Although the shapes of the multi-colored lines in Fig. 13 are critically dependent on x, the rest of the diagram does not appear to change with x, at least over the limited range of x used in Fig. 13. The almost-circular blue line in Fig. 13 has previously been seen in Fig. 2 in results from Mie calculations. The explanation of this feature becomes obvious in Fig. 13: it is simply the locus of the end-points of the Debye series calculations when p_{max} is sufficient to replicate the Mie result in the vicinity of the resonance.

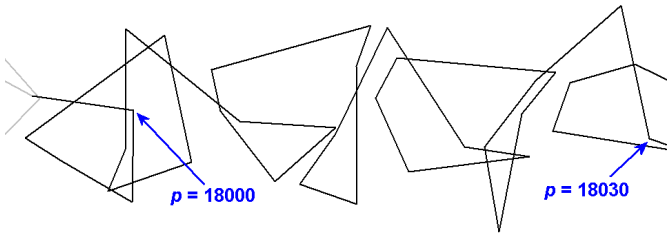

Fig. 12 A magnified view of the "straight line" in Fig. 11(a) in the vicinity of p ≈ 18,000 using a magnification factor of 10^5. Although the phases of the individual scattering contributions vary wildly, the horizontal line in Fig. 11(a) extending to the right towards the Mie result indicates that the average phase is close to 0°.

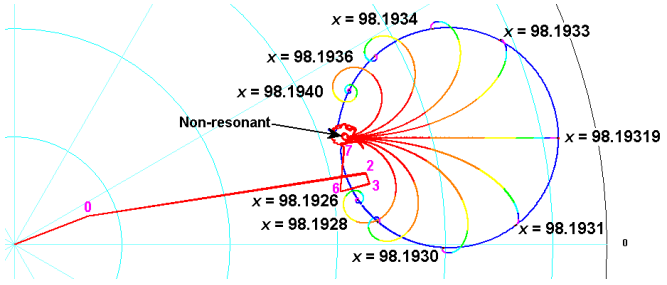

Fig. 13 As Fig. 11(a) except that it shows results for selected values of x around the resonance at x = 98.19319. The dominant contributions to non-resonant scattering are marked by the values of p = 0, 2, 3, 6 and 7. The blue almost-circular feature shows the locus of the Mie results as seen in Fig. 2.

In Fig. 13, the resonance at $x = 98.19319$ is at the extreme right of the almost-circular feature. However, Fig. 2 reminds us that some resonances (e.g. at $x = 98.99$) are on the extreme left of the almost-circular feature. This difference is caused by the $\tau_n(\theta)$ term in Eq. (1): for TE resonances, increasing p causes the horizontal straight lines to extend to the right when $\tau_n(\theta) > 0$ and to the left when $\tau_n(\theta) < 0$.

5. THE ROLE OF $R^{121}{}_n$ IN RESONANCES

Fig. 11 indicates that the Mie resonances of order n are caused by the Debye series terms of order n for $p > 0$ being in phase with each other. In Eq. (4) for the Debye series, the expression $-T^{21}{}_n\ (R^{121}{}_n)^{p-1}\ T^{12}{}_n$ for $p > 0$ corresponds to transmission through the sphere with $p - 1$ internal reflections. Note that all of these coefficients ($T^{21}{}_n$ $T^{12}{}_n$ and $R^{121}{}_n$) are represented by complex numbers. To achieve resonance, each $p + 1$ term must be in phase with the p term, which implies that $R^{121}{}_n$ must be positive and real (i.e. the imaginary part of $R^{121}{}_n$ must be zero).

This differs from the widely accepted criterion [3, 6, 7, 23, 24] that TE resonances of order n occur at the value of x where the real part of b_n is 1 and imaginary part of b_n is zero. Given this discrepancy, it is worth examining some numerical results: The two multi-colored lines in Fig. 14 show the Debye series approximations to the Mie results for b_{110} as p is increased from zero to 20,000 for $x = 98.1931901251548$ where $\mathrm{Im}(b_{110}) = 0$ and for $x = 98.19319011687$ where $\mathrm{Im}(R^{121}{}_{110}) = 0$. Both lines start at $b_{110} = 1.37\times10^{-4} + i\ 4.64\times10^{-5}$ when $p = 0$, but they diverge as p increases. The upper line curves towards $b_{110} = 1$, whereas the lower line is straight because all of the terms are in phase when $p > 1$. The vertical scale in Fig. 14 has been greatly exaggerated to highlight the differences in these curves. It also demonstrates the "horizontal" straight lines noted in Figs. 11 and 13 are not quite horizontal: in this case, the difference is 0.0053° which is caused by the product $-T^{21}{}_{110}\ T^{12}{}_{110}$ in Eq. (4).

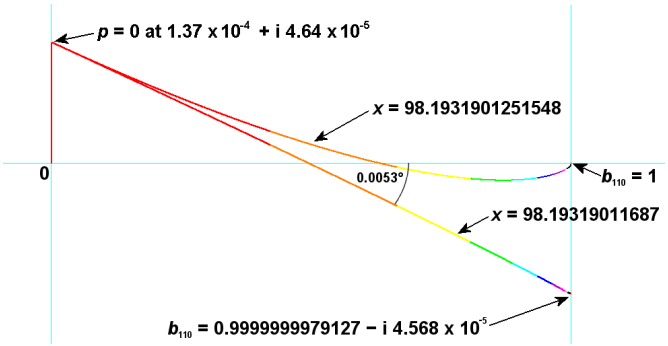

Fig. 14 Cumulative results from Debye series calculations of b_{110} for $p = 0$ through $p = 20{,}000$ for $x = 98.1931901251548$ where $\mathrm{Im}(b_{110}) = 0$ and for $x = 98.19319011687$ where $\mathrm{Im}(R^{121}{}_{110}) = 0$. The vertical scale representing the imaginary values of b_{110} has been exaggerated by a factor of 5,000 to highlight the differences between the two curves.

There is no practical difference in the values of x predicted by the two criteria of $\mathrm{Im}(b_n) = 0$ and $\mathrm{Im}(R^{121}{}_n) = 0$. Nevertheless, the criterion based on $R^{121}{}_n$ seems preferable because the concept of resonance is intrinsically linked to many terms being in phase with each other. Furthermore, as shown below, various characteristics of resonances are dependent on $R^{121}{}_n$.

Increasing p by 1 reduces the scattered amplitude by the factor of $|R^{121}{}_n|$, as indicated in Table 1 using the calculated numerical value of $R^{121}{}_{110} \approx 0.999727$ corresponding to the resonance at $x = 98.19319$ where $n = 110$ and $l = 3$.

Table 1 Relative amplitudes of the p terms when $|R^{121}{}_n| = 0.999727$.

p	$\lvert R^{121}{}_n\rvert^{p-1}$
1	0.999727
2	0.999454
10	0.997273
100	0.973061
1,000	0.761026
5,000	0.255268
10,000	0.065162
20,000	0.004246

Although Table 1 shows that $|R^{121}{}_n|^{p-1}$ becomes very small for large values of p, Eq. (4) shows that the Mie result is proportional to the sum to infinity of this geometric progression. As discussed in Sec. 3, it is useful to know how many terms of the Debye series are needed to replicate the Mie result. For example, if we want the amplitude of the Debye series result to be a fraction k of the amplitude of the Mie result at resonance, the required number of terms p_{max} is given by:

$$p_{max} \approx \log[1 - k] / \log[|R^{121}{}_n|] \qquad (5)$$

Applying Eq. 5 for $k = 0.99$ at each of the resonances shown in Fig. 1 gives the results shown in Table 2. The calculated values of $p_{max} = 268$ and $p_{max} = 16{,}683$ for the first two resonances listed in Table 2 are consistent with the estimates from Fig. 6 of $p_{max} \approx 200$ and $p_{max} > 10{,}000$ respectively. Table 2 also indicates that $R^{121}{}_n$ decreases as l increases, resulting in extremely high values of p_{max} for the two resonances with $l = 1$.

Lock [9] noted that the width δx (FWHM) of the amplitude of the resonance can be calculated by:

$$\delta x = 4 \arcsin\left[(1 - |R^{121}{}_n|)/2 \times \sqrt{(3/|R^{121}{}_n|)}\right] \qquad (6)$$

Having determined δx, it is simple to determine the Q factor for each resonance using the relationship $Q = x/\delta x$. For example, looking at the resonances listed in Table 2, the calculated values of Q vary between 1,650 (for $n = 105$ and $l = 4$) and 5.73×10^{11} (for $n = 124$ and $l = 1$).

Table 2 Calculations of p_{max} and Q for the resonances listed in Fig. 1

x	n	l	$\lvert R^{121}{}_n \rvert$	p_{max} for $k = 0.99$	Q
98.13119	105	4	0.982977088896	268	1,650
98.19319	110	3	0.999726949302	16,863	1.04E+05
98.47316	116	2	0.999999428669	8.06E+06	4.98E+07
98.50970	123	1	0.999999999936	7.23E+10	4.44E+11
98.94137	106	4	0.984903176617	303	1,878
98.98997	111	3	0.999768766066	19,913	1.24E+05
99.25671	117	2	0.999999533135	9.86E+06	6.14E+07
99.27838	124	1	0.999999999950	9.15E+10	5.73E+11
99.75111	107	4	0.986634116076	342	2,140
99.78645	112	3	0.999804341222	23,534	1.47E+05

It is important to recognize that the results shown in Table 2 represent ideal results. For example, the calculations assume that the spherical particle is assumed to be non-absorbing (i.e. the imaginary part of the refractive index is zero). Any absorption within the particle would reduce the value of $R^{121}{}_n$, thus reducing the values of p_{max} and Q. Furthermore, as shown in [25, 26], the quality of resonances can be degraded by various other "real-world" mechanisms.

6. CONCLUSIONS

As Mie resonances are caused by the combined effects of many terms in the Debye series, it is not obvious how the Debye series can be used to analyze these resonances. This paper uses the Debye series to reveal much interesting information about resonances. For example, Fig. 8 shows that the Debye series contributions vary rapidly in phase in the vicinity of resonances, tending to congregate around 0°. The effects of this behavior can also be seen in Mie results: the near-circular loops shown in Fig. 2 can be explained by the Debye series results in Fig. 13.

More importantly, this paper demonstrates that the Debye series expansion in Eq. (4) provides a direct and succinct explanation for these resonances: in particular, resonances for a specified value of n occur when the term $R^{121}{}_n$ is positive and real. This criterion ensures that contributions from partial wave n to the scattered field from Debye series terms from $p = 1$ through $p = \infty$ are precisely in phase, thus causing the resonance.

The value of $\lvert R^{121}{}_n \rvert$ at the resonance also determines the number of terms p_{max} in the Debye series that are required to approximate the Mie solution: the examples in this paper show that some broad resonances require only a few hundred terms, whilst very narrow resonances can require billions of terms. Similarly, the widths δx of the resonances and their corresponding Q factors can easily be calculated from $\lvert R^{121}{}_n \rvert$.

Acknowledgements The author thanks J. A. Lock for his valuable comments on an early version of this manuscript.

Disclosures. The author declares no conflicts of interest.

Data availability Data underlying the results presented in this paper are not publicly available at this time but may be obtained from the author upon reasonable request.

REFERENCES

1. H. C. Bryant and A. J. Cox, "Mie Theory and the Glory," J. Opt. Soc. Am. **56**, 1529-1532 (1966).
2. T. S. Fahlen and H. C. Bryant, "Optical Back Scattering from Single Water Droplets," J. Opt. Soc. Am. **58**, 304-310 (1968).
3. P. Chýlek, "Partial-wave resonances and the ripple structure in the Mie normalized extinction cross section," J. Opt. Soc. Am. **66**, 285-287 (1976).
4. P. Chýlek, J. T. Kiehl, and M. K. W. Ko, "Narrow resonance structure in the Mie scattering characteristics," Appl. Opt. **17**, 3019-3021 (1978).
5. P. Chýlek, J. T. Kiehl, and M. K. W. Ko, "Optical levitation and partial wave resonances," Phys. Rev. A **18**, 2229-2233 (1978).
6. P. R. Conwell, P. W Barber, and C. K. Rushforth, "Resonant spectra of dielectric spheres," J. Opt. Soc. Am. A **1**, 62-67 (1984).
7. J. R. Probert-Jones, "Resonance component of backscatter by large dielectric spheres," J. Opt. Soc. Am. A **1**, 822-830 (1984).
8. S. C. Hill and R. E. Benner, "Morphology-dependent resonances associated with stimulated processes in microspheres," J. Opt. Soc. Am. B **3**, 1509-1514 (1986).
9. J. A. Lock, "Cooperative effects among partial waves in Mie scattering," J. Opt. Soc. Am. A **5**, 2032-2044 (1988).
10. S. C. Hill and R. E. Benner, "Morphology-dependent resonances" in *Optical effects associated with small particles*, P. W. Barber and R. K. Chang (Eds.), World Scientific, Singapore (1988).
11. P. Chýlek, "Resonance structure of Mie scattering: distance between resonances," J. Opt. Soc. Am. A **7**, 1609-1613 (1990).
12. C. C. Lam, P. T. Leung, and K. Young, "Explicit asymptotic formulas for the positions, widths and strengths of resonances in Mie scattering," J. Opt. Soc. Am. B **9**, 1585-1592 (1992).
13. L. G. Guimarães and H. M. Nussenzveig, "Theory of Mie resonances and ripple fluctuations," Opt. Commun. **89**, 363–369 (1992).
14. L. G. Guimarães, "Theory of Mie caustics," Opt. Commun. **103**, 339-344 (1993).
15. S. Schiller, "Asymptotic expansion of morphological resonance frequencies in Mie scattering," Appl. Opt. **32**, 2181-2185 (1993).
16. B. R. Johnson, "Theory of morphology-dependent resonances: shape resonances and width formulas," J. Opt. Soc. Am. A **10**, 343-352 (1993).
17. L. G. Guimarães and H. M. Nussenzveig, "Uniform approximation to Mie resonances," J. Mod. Opt. **41**, 625-647 (1994).
18. G. Videen, J. Li, and P. Chýlek, "Resonances and poles of weakly absorbing spheres," J. Opt. Soc. Am. A **12**, 916-921 (1995).
19. M. I. Mishchenko, L. D. Travis and A.A. Lacis, Scattering, Absorption and Emission of Light by Small Particles, Cambridge University Press (2002) https://pubs.giss.nasa.gov/books/2002_Mishchenko_mi06300n/.
20. P. Debye, "Das Elektromagnetische Feld um einen Zylinder und die Theorie des Regenbogens," Phys. Zeit. **9**:775-778 (1908), reprinted and translated into English in pp. 198–204 of *Geometrical aspects of scattering*, P. L. Marston (Ed.), MS89, SPIE Press (1994).
21. E. A. Hovenac and J. A. Lock, "Assessing the contributions of surface waves and complex rays to far-field Mie scattering by use of the Debye series," J. Opt. Soc. Am. A **9**, 781-795 (1992).
22. J. A. Lock and P. Laven, "The Debye Series and its use in Time-Domain Scattering" in *Light Scattering Reviews Vol. 11*, A. Kokhanovsky (Ed.), Springer Praxis (2016).
23. G. J. Rosasco and H. S. Bennett, "Internal field resonance structure: Implications for optical absorption and scattering by microscopic particles," J. Opt. Soc. Am. **68**, 1242-1250 (1978).
24. G. C. Gaunaurd, H. Überall, and A. Nagl, "Complex-frequency poles and creeping-wave transients in electromagnetic-wave scattering," Proc. IEEE **71**, 172-174 (1983).
25. A. L. Huston, H.-B. Lin, J. D. Eversole, and A. J. Campillo, "Effect of bubble formation on microdroplet cavity quality factors," J. Opt. Soc. Am. B **13**, 521-531 (1996).
26. M. L. Gorodetsky, A. A. Savchenkov, and V. S. Ilchenko, "Ultimate Q of optical microsphere resonators," Opt. Lett. **21**, 453-455 (1996).